Physics and Imaging in Radiation Oncology 30 (2024) 100584

Contents lists available at ScienceDirect

Physics and Imaging in Radiation Oncology

journal homepage: www.sciencedirect.com/journal/physics-and-imaging-in-radiation-oncology

Original Research Article

Optimized raw data selection for artifact reduction of breathing controlled four-dimensional sequence scanning

Juliane Szkitsak [a,b], Andre Karius [a,b], Susanne Fernolendt [c], Philipp Schubert [a,b], Stefan Speer [a,b], Rainer Fietkau [a,b], Christoph Bert [a,b,*], Christian Hofmann [a,c]

[a] Department of Radiation Oncology, Universitätsklinikum Erlangen, Friedrich-Alexander-Universität Erlangen-Nürnberg, Erlangen, Germany
[b] Comprehensive Cancer Center Erlangen-EMN (CCC ER-EMN), Erlangen, Germany
[c] Siemens Healthcare GmbH, 91301 Forchheim, Germany

ARTICLE INFO

Keywords:
4DCT
Irregular breathing
Artifacts
Optimized raw data selection
Hysteresis
Reconstruction

ABSTRACT

Background and purpose: Even with most breathing-controlled four-dimensional computed tomography (4DCT) algorithms image artifacts caused by single significant longer breathing still occur, resulting in negative consequences for radiotherapy. Our study presents first phantom examinations of a new optimized raw data selection and binning algorithm, aiming to improve image quality and geometric accuracy without additional dose exposure.

Materials and methods: To validate the new approach, phantom measurements were performed to assess geometric accuracy (volume fidelity, root mean square error, Dice coefficient of volume overlap) for one- and three-dimensional tumor motion trajectories with and without considering motion hysteresis effects. Scans without significantly longer breathing cycles served as references.

Results: Median volume deviations between optimized approach and reference of at maximum 1% were obtained considering all movements. In comparison, standard reconstruction yielded median deviations of 9%, 21% and 12% for one-dimensional, three-dimensional, and hysteresis motion, respectively. Measurements in one- and three-dimensional directions reached a median Dice coefficient of 0.970 ± 0.013 and 0.975 ± 0.012, respectively, but only 0.918 ± 0.075 for hysteresis motions averaged over all measurements for the optimized selection. However, for the standard reconstruction median Dice coefficients were 0.845 ± 0.200, 0.868 ± 0.205 and 0.915 ± 0.075 for one- and three-dimensional as well as hysteresis motions, respectively. Median root mean square errors for the optimized algorithm were 30 ± 16 HU^2 and 120 ± 90 HU^2 for three-dimensional and hysteresis motions, compared to 212 ± 145 HU^2 and 130 ± 131 HU^2 for the standard reconstruction.

Conclusions: The algorithm was proven to reduce 4DCT-related artifacts due to missing projection data without further dose exposure. An improvement in radiotherapy treatment planning due to better image quality can be expected.

1. Introduction

Radiation therapy of thoracic and abdominal tumors is affected by internal target and organ motion caused by breathing. To compensate corresponding movements, motion management strategies are required [1]. An essential part is four-dimensional (4D) computed tomography (CT) [2]. 4DCT provides breathing-phase specific snapshots of the patient anatomy and therefore valuable information regarding tumor shape and motion. Based on 4D CT, the Internal Target Volume (ITV) can be defined as introduced by the International Commission on Radiation Units and Measurements (ICRU) [3] to integrate time-resolved image information of the individual breathing phases into the target volume [4]. This strategy of passive movement management is suitable for small periodic movements (≤5 mm) and of particular importance in extracranial stereotactic body radiotherapy [4].

However, conventional 4DCT images are often affected by artifacts due to irregular breathing like anatomical deformations, as well as double or incomplete structures, leading to delineation errors [5–8] and incorrect dose calculations [7,9]. The presence of image artifacts in 4DCT data used for stereotactic treatment planning of lung and liver

* Corresponding author at: Universitätsklinikum Erlangen, Universitätsstraße 27, 91054 Erlangen, Germany.
E-mail address: Christoph.Bert@uk-erlangen.de (C. Bert).

https://doi.org/10.1016/j.phro.2024.100584
Received 8 January 2024; Received in revised form 10 April 2024; Accepted 2 May 2024
Available online 5 May 2024

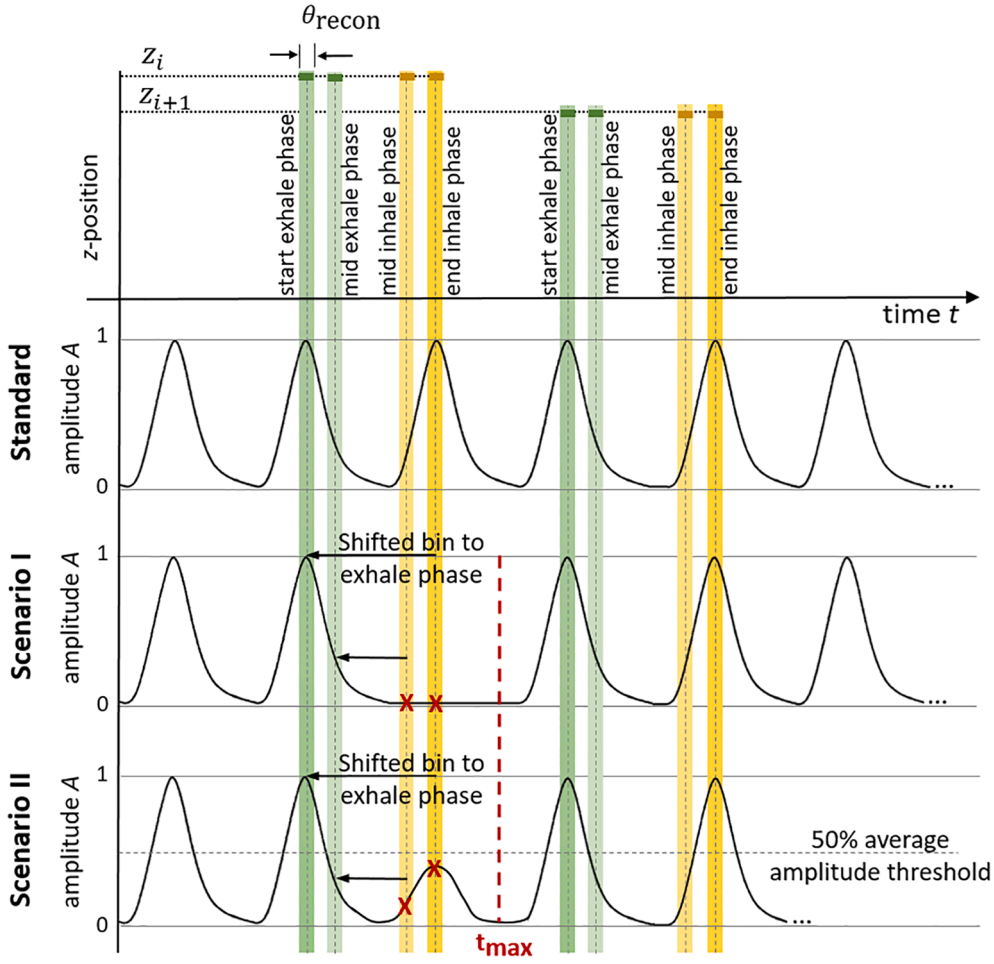

Fig. 1. Schematic representation of the optimized binning approach for optimized raw data selection. Standard shows the selection of binning time points with regular breathing pattern. θ_{recon} describes the area that is standardly used for reconstruction at a defined table position and for a defined breathing phase. Scenario I and II demonstrate selection of binning points if inspiration information is missing or insufficient (marked with red cross). (For interpretation of the references to colour in this figure legend, the reader is referred to the web version of this article.)

metastasis has a negative impact on clinical outcome [10].

To counteract breathing-related artifacts, real-time signal analysis was proposed to control projection data acquisition in a prospective way [11,12]. By adapting the scanning process individually to the actual breathing pattern, Werner *et al.* presented a hybrid approach combining optimized prospective scan triggering and retrospective projection data selection [13,14]. *In-silico*, phantom, and patient data evaluations demonstrated significant reductions of image artifacts due to irregular breathing compared to conventional spiral 4DCT [14–16]. A profound quality assurance of this approach was published recently [17].

In most cases, online analysis of the actual breathing cycle can ensure sufficient projection data coverage and thus avoid corresponding artifacts. However, even with the hybrid algorithm artifacts could not be avoided completely [15,16]. In this respect, a remaining fraction of CT images (~2–5%) suffered from a relevant loss of anatomical information. Due to radiation protection reasons, a maximum scan time t_{max} per table position is set depending on the breathing frequency. Thus, if the patient exhales for too long or the amplitude of the inspiration is too low compared to the reference cycle, no or not enough inspiration information may be acquired. A rescan can counteract this issue at the respective table position [8], resulting in longer scan times and additional radiation exposure [11,13].

In this paper, we propose a new binning selection approach to counteract artifacts without additional dose exposure that can improve planning CT quality for intra-fractionally moving tumors. Missing inspiration data are replaced by respective expiration data. The aim of this work was to evaluate image quality and geometric accuracy based on phantom measurements considering motion trajectories with and without hysteresis. Additionally, first patient data are exemplarily demonstrated and discussed.

2. Materials and methods

2.1. Breathing controlled 4DCT algorithm and optimized raw data selection

Based on a reference cycle of the patient's breathing pattern, scan parameters (e.g. gantry rotation time) are automatically and individually selected. Subsequently, the CT data acquisition is performed in sequence scanning mode, controlled and monitored by an online real-time breathing signal analysis. When a pre-set level of similarity between actual and reference breathing cycle is reached, the beam is switched on immediately before maximum inhalation. Projection data are acquired continuously at a defined z-position until a complete breathing cycle is covered. When sufficient projection data coverage is achieved, the acquisition is stopped and the table is moved to the next z-position. The scanning procedure is repeated until the whole scan range is covered. For details regarding the algorithm, see [13].

In order to ensure that the individual adjustment of the scan length results in an unacceptably high dose exposure, the acquisition time at distinct table positions is, due to radiation protection reasons, limited to a maximum time t_{max} by the algorithm, depending on breathing

Table 1
Overview of the selected parameters of the phantom measurements. Each measurement was performed with and without one excessive breathing pauses at maximum exhalation. All measurements were repeated three times.

	Function	Amplitude			Frequency
		Superior-Inferior	Anterior-Posterior	Lateral	
1D movement	Without hysteresis/ Cos^6-function	20 mm	–	–	0.2 s^{-1}
		15 mm	–	–	
		10 mm	–	–	
		5 mm	–	–	
3D movement	Without hysteresis/ Cos^6-function	20 mm	7 mm	7 mm	0.2 s^{-1}
		15 mm	5 mm	5 mm	
		10 mm	3 mm	3 mm	
		5 mm	1 mm	1 mm	
	With hysteresis/ Sin-function	20 mm	7 mm	7 mm	0.2 s^{-1}
		15 mm	5 mm	5 mm	
		10 mm	3 mm	3 mm	
		5 mm	1 mm	1 mm	

frequency. This might lead to artifacts, if not enough projection data about the whole breathing cycle are acquired within this time. To minimize these artifacts without applying additional dose, an algorithm to optimize raw data selection was developed, aiming to replace missing inspiration data by respective expiration data. There are two typical scenarios (see also Fig. 1):

Scenario I: Due to a too long exhalation phase, the maximum scan time t_{max} is reached at a defined z-position before the inhalation phase has started. Thus, inspiration data is completely missing, resulting in strong step artifacts depending on the amplitude.

Scenario II: To avoid artifacts due to a too low inspiration amplitude, the i4DCT algorithm detects amplitudes $< 50\%$ of the reference breathing cycle and continues data acquisition. The acquisition is terminated either by detecting an amplitude $\geq 50\%$ within t_{max} or by reaching t_{max}, resulting in absence of sufficient inspiration information at defined table position.

For these two scenarios, the binning, and thus the used projection data for reconstruction, was adapted. Instead of using the local minimum and maximum of the inspiration phase and the corresponding amplitude values between these two points as described in [18], only the expiration phase is considered to calculate the binning time points t_{bin}. The inspiration binning points thus match those of the expiration. Fig. 1 shows schematically how the binning points are set in these two scenarios. Subsequently, CT data is retrospectively sorted, assigned to the different breathing phases and reconstructed, resulting in a 3DCT for defined breathing phase.

2.2. CT data and breathing motion acquisition

CT data were acquired with the breathing controlled 4DCT algorithm (referred to as "i4DCT"), implemented on the SOMATOM go.Open Pro Scanner (Siemens Healthineers AG, Forchheim, Germany). Scan and reconstruction parameters were 120 kV tube voltage, 0.9x64x0.6 mm table increment and a Qr40 kernel. 10-phase-images were reconstructed amplitude-based. The reconstruction of the raw data was retrospectively performed using a research reconstruction software provided by Siemens which enables the option of optimized binning selection.

The Respiratory Gating for Scanners system (RGSC, Varian Medical Systems, Inc. Palo Alto, USA) was used for respiratory signal acquisition. It consists of a table-mounted infrared (IR) camera and a marker block with passive IR reflectors. The respiratory curve was transferred to the CT scanner in real-time and used as input for the i4DCT algorithm.

2.3. Motion measurements

The Dynamic Thorax Motion Phantom Model 008A (Computerized Imaging Reference System (CIRS), Norfolk, USA) was used for phantom measurements, providing a motion accuracy and reproducibility of $\pm$ 0.1 mm [19]. A spherical insert with 30 mm diameter, 0.2 s^{-1} motion frequency, and a cos^6-motion-function, like in other publications [20–22], was chosen to simulate a realistic clinical scenario. Selection of breathing amplitudes was based on previously published patient studies [9,23]. Phantom movements were performed both in one- and three-dimensional directions. Additionally, three-dimensional measurements were performed with and without phantom's hysteresis function, which had to be conducted with sinusoidal curves. An overview of the chosen parameters can be found in Table 1.

Furthermore, two different measurements were performed for each selected combination of movement direction and breathing amplitude. First, a standard 4DCT scan without breathing pauses served as ground truth ($4DCT_{Ref}$). Second, the phantom movement was stopped at maximum expiration, simulating an excessively long exhalation. Once the data acquisition had stopped, since $t_{acquisition} \geq t_{max}$, the table moved to the next position, the phantom movement was restarted, and the data acquisition continued. The data of the second measurement were reconstructed by using both the standard ($4DCT_{Standard}$) and optimized raw data selection ($4DCT_{Optimized}$). In the following, $4DCT_{Standard}$ and $4DCT_{Optimized}$ together are summarized as $4DCT_{Rekon}$. Since the above mentioned scenario I presents the worst case, investigations were focused on this case. All measurements were repeated three times.

2.4. Data analysis

The segmentation of the spherical insert was performed using a threshold-based method described in [17]. Based on this, image quality and geometric accuracy of the standard and optimized reconstruction were evaluated. First, the spherical volume was examined in comparison to the reference scan $4DCT_{Ref}$ separately for each respiration phase. Furthermore, to obtain a reliable conclusion about the functionality of the algorithm even in case of tumor trajectory hysteresis, the Dice similarity coefficient (DSC) between $4DCT_{Ref}$ and $4DCT_{Rekon}$ was calculated as recommended in [24]. Similarity between $4DCT_{Ref}$ and $4DCT_{Rekon}$ was additionally evaluated for each individual breathing phase using the Root Mean Square Error (RMSE), defined as

$$RMSE = \sqrt{\frac{1}{n}\sum_{i=1}^{n}\left(4DCT_{Ref}(i) - 4DCT_{Rekon}(i)\right)^2} \quad (1)$$

Here, n represents the number of all voxels of the scan and $4DCT_{Ref/\ Rekon}(i)$ the CT numbers of the i-th voxel of the corresponding scans, respectively. Since the binning time points of the expiration are the same in optimized and standard reconstruction, only the inspiration phases were observed. For clarity, only the 0%, 40% and 80% of the inspiration are presented in the following. Statistical significance was

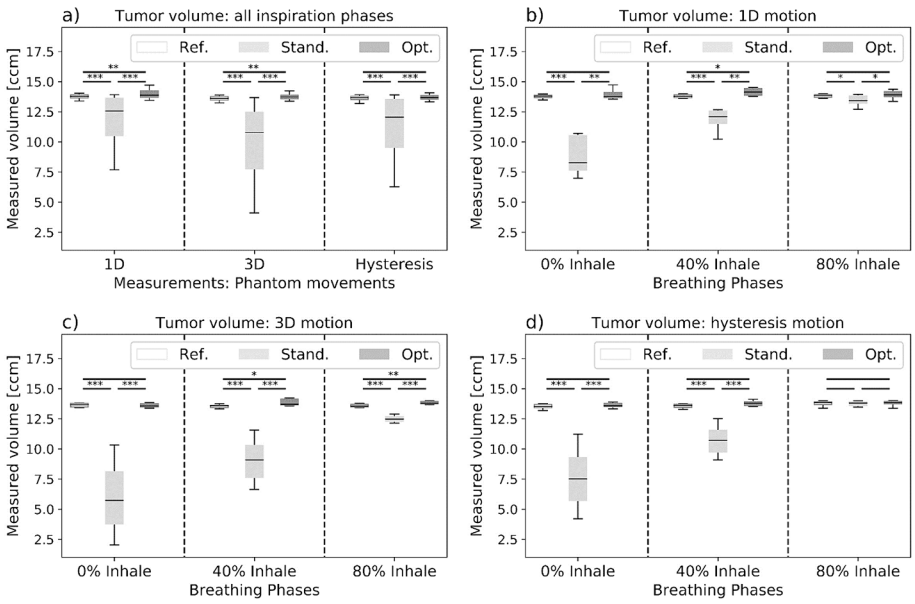

Fig. 2. Tumor volume deviations for phantom measurements. (a) shows the results for all breathing phases for the reference scan without breathing pause as well as the standard and the optimized reconstruction for breathing curves with a significant longer exhalation. Deviations for (b) one-dimensional, (c) three-dimensional, and (d) hysteresis motion for different breathing phases are demonstrated. In the boxplots, the horizontal lines indicate the median, boxes the interquartile range, and the whiskers the 95th percentile of the results. Outliers are not shown for clarity. ($p < 0.05$, **: $p < 0.01$, ***: $p < 0.001$).

tested with Wilcoxon-signed-rank test for independent samples.

2.5. Patient data

Finally, the effect of the optimized binning on patient data is exemplarily demonstrated and discussed. For this purpose, the patient's breathing curves with standard and optimized binning time points and corresponding CT images are presented for a patient with $t_{acquisition} \geq t_{max}$. Again, only a worst-case scenario was considered, i.e. no information about the inspiration phase was available. All procedures performed were in accordance with the ethical standards of the institutional research committee and with the 1964 Helsinki declaration and its later amendments. Patient consent was not required for this retrospective study per local regulatory policies.

3. Results

3.1. Phantom data

Considering the phantom study, examinations with one- and three-dimensional motions without hysteresis showed significant improvements of image quality and geometrical accuracy compared to the standard reconstruction (see videos in Supplementary Material A). 4DCT-related step artifacts, resulting from missing inspiration data,

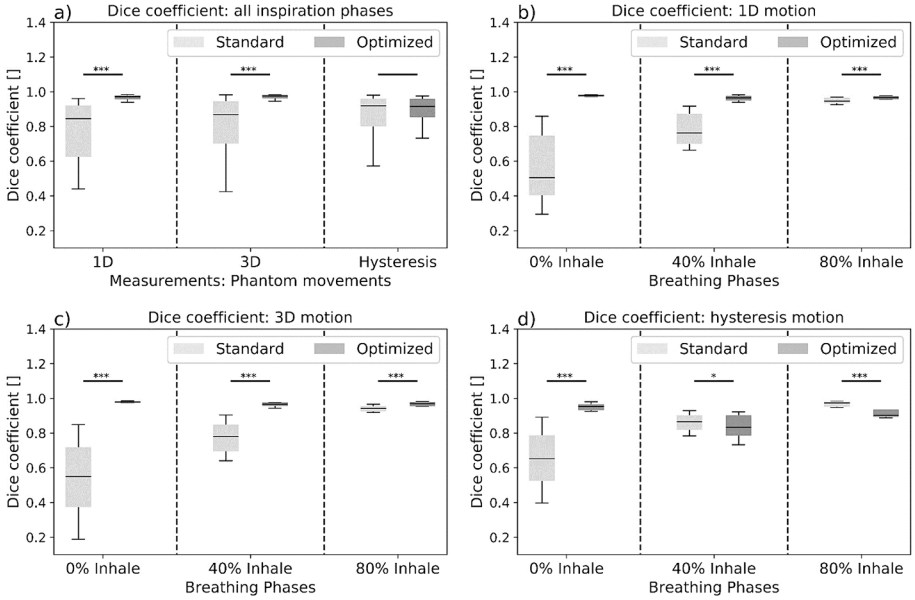

Fig. 3. Deviations from Dice coefficient for phantom measurements. (a) shows the results for all breathing phases for the reference scan without breathing pause as well as the standard and the optimized reconstruction for breathing curves with a significant longer exhalation. Deviations for (b) one-dimensional, (c) three-dimensional and (d) hysteresis motion for different breathing phases are demonstrated. ($p < 0.05$, **: $p < 0.01$, ***: $p < 0.001$).

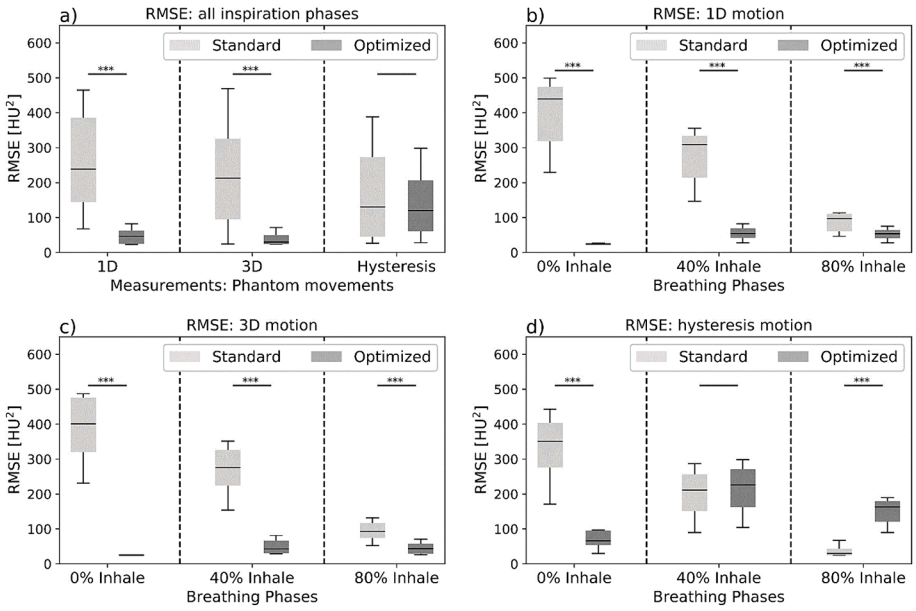

Fig. 4. Deviations from root mean square error for phantom measurements. (a) shows the results for all breathing phases for the reference scan without breathing pause as well as the standard and the optimized reconstruction for breathing curves with a significant longer exhalation. Deviations for (b) one-dimensional, (c) three-dimensional and (d) hysteresis motion for different breathing phases are demonstrated. ($p < 0.05$, **: $p < 0.01$, ***: $p < 0.001$).

were avoided by using the optimized binning approach. Although partially statistically significant differences between $4DCT_{Optimized}$ and $4DCT_{Ref}$ were observed, they were out of clinical relevance. Phantom measurements with hysteresis were in good agreement with one- and three-dimensional motions without hysteresis concerning the correct representation of the spherical insert. However, differences in the trajectory between expiration and inspiration led to substantial differences compared to $4DCT_{Ref}$ and thus a reduced Dice coefficient.

A more detailed analysis revealed a median volume deviation between $4DCT_{Ref}$ und $4DCT_{Optimized}$ of maximum 1% (corresponding to 0.14 cm^3) for all movement directions (see Fig. 2). Significant differences were observed for one- and three-dimensional motions ($p < 0.01$). In comparison, $4DCT_{Standard}$ yielded a median deviation of 9%, 21% and 12% for one-dimensional, three-dimensional and hysteresis motion, respectively, compared to $4DCT_{Ref}$ ($p < 0.001$). Maximum volume deviation was 11.75 cm^3 for $4DCT_{Standard}$ and 1.41 cm^3 for $4DCT_{Optimized}$. The occurrence of such artifacts in standard reconstructions led to the aforementioned enhanced volume differences, which were largest at the beginning of inspiration and reduced when reaching the maximum inspiration. This behavior was observed for all measurements. When inspiration projection data were missing, the standard reconstruction used the acquired data shortly before first maximum to distribute binning points (see Fig. 5, "standard binning selection"). Consequently, provided data at the acquisition start was not enough for artifact-free reconstruction at a certain z-position, resulting in discrepancies due to different breathing phases compared to previous and following detector positions.

In contrast to the volume, Dice coefficient analyses pointed out the impact of hysteresis on the geometric accuracy achieved with the optimized binning approach (see Fig. 3). Measurements in one- and three-dimensional directions reached a median Dice coefficient of 0.970 ± 0.013 and 0.975 ± 0.012, respectively, but only 0.918 ± 0.075 for hysteresis motion averaged over all measurements for $4DCT_{Optimized}$. Measurements with maximum hysteresis revealed the lowest Dice coefficient of 0.713. However, for $4DCT_{Standard}$ median Dice coefficients were only 0.845 ± 0.200, 0.868 ± 0.205 and 0.915 ± 0.075 for one- and three-dimensional as well as hysteresis, respectively. Differences between $4DCT_{Optimized}$ and $4DCT_{Standard}$ were significant for one- and three-dimensional motions ($p < 0.001$) but not for hysteresis motion ($p > 0.05$). Regarding hysteresis motions, both scanning approaches were thus suited similarly to achieve imaging fidelity, while $4DCT_{Optimized}$ showed substantial improvements regarding all motions without hysteresis.

Similar to the volume, the Dice coefficient changed over the respiratory cycle for $4DCT_{Standard}$ due to the same aforementioned reasons. For instance, DSC was 0.504 ± 0.222 for 0% inspiration, to 0.762 ± 0.132 for 40% inspiration and 0.945 ± 0.945 for 80% inspiration for one-dimensional movement. Additionally, difference between certain respiratory phases for $4DCT_{Optimized}$ can be observed as well (see Fig. 3d). Due to the variations in the trajectories of the spherical insert between inspiration and expiration, considering hysteresis motions and the corresponding disability of the algorithm to address this effect, the described differing results depending on the breathing phase occurred (see Fig. 5, phantom data with new binning approach). The larger the Euclidean distance between the insert positions at the different time points of the movement (mid-inspiration compared to mid-exhalation) was, the smaller was also the overlapping volume, resulting in a lower Dice coefficient. Median Dice coefficient varied from 0.953 ± 0.021 (0% inspiration) to 0.833 ± 0.080 (40% inspiration) to 0.902 ± 0.025 (80% inspiration) for hysteresis reconstructed with $4DCT_{Optimized}$.

Confirmation of these findings was provided by the RMSE analyses. The corresponding results were in good agreement between $4DCT_{Ref}$ and $4DCT_{Optimized}$ for one- and three-dimensional measurements. On the other hand, for hysteresis motions larger deviations were observed (see Fig. 4). To be concrete, the median RMSE of $4DCT_{Optimized}$ was 46 ± 20 HU^2, 30.0 ± 16 HU^2 and 120 ± 90 HU^2 for 1D, 3D and hysteresis motion, respectively. In comparison, median RMSE of $4DCT_{Standard}$ was 238 ± 139 HU^2, 212 ± 145 HU^2 and 130 ± 131 HU^2. Differences between $4DCT_{Standard}$ and $4DCT_{Optimized}$ were significant for 1D and 3D motion (p-value < 0.001).

The RMSE results thus showed again a typical pattern for the optimized and standard reconstruction. While the RMSE for the standard reconstruction decreased with increasing inspiration, RMSE for optimized reconstruction was largest at 40% inspiration. For hysteresis motions, the median RMSE was 350 ± 105 HU^2 and 66 ± 26 HU^2 (0% inspiration), 211 ± 76 HU^2 and 226 ± 83 HU^2 (40% inspiration) as well as 30 ± 17 HU^2 and 162 ± 47 HU^2 (80% inspiration) for $4DCT_{Standard}$ and $4DCT_{Optimized}$, respectively. Differences between both

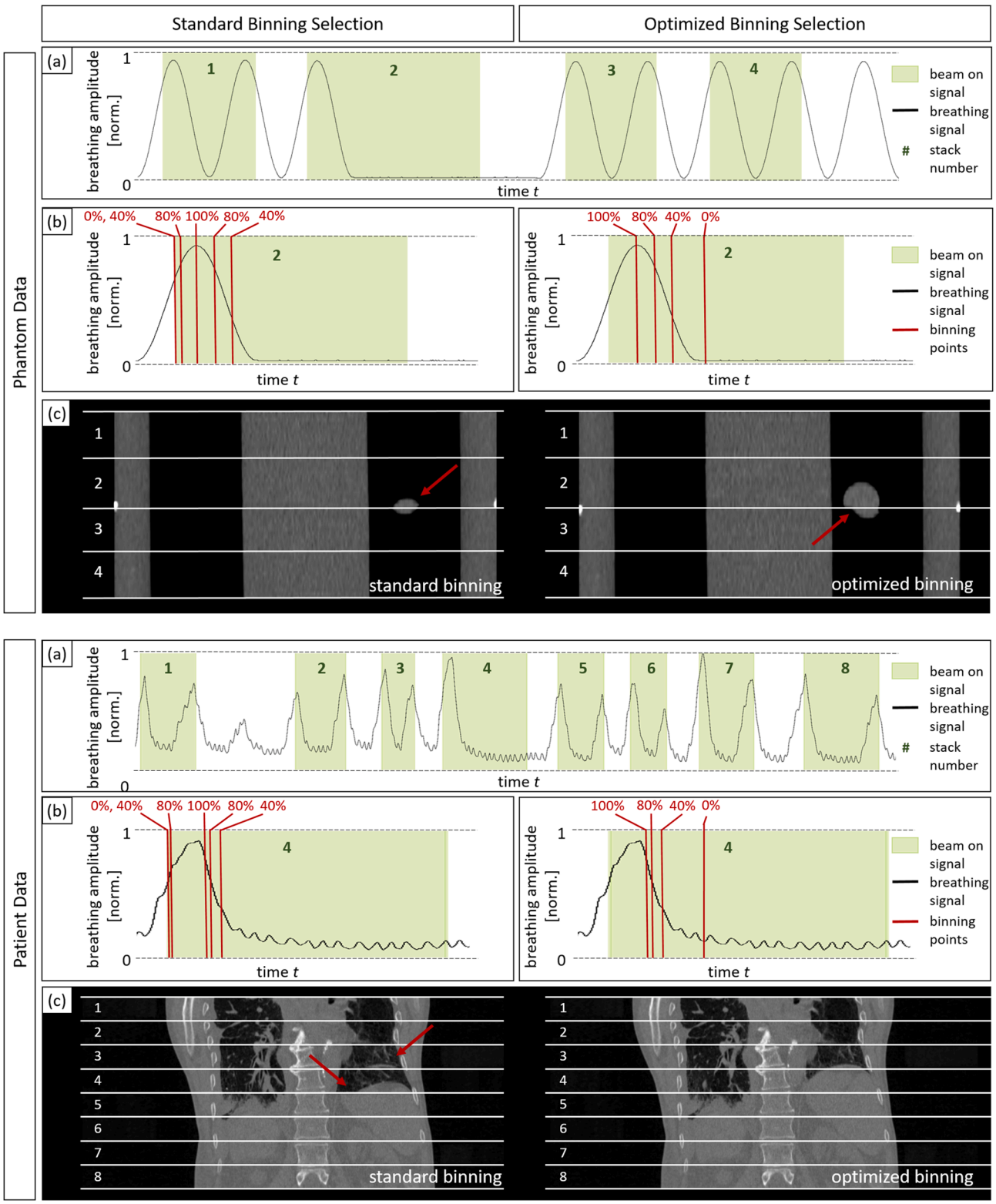

Fig. 5. Schematic representation of the standard (left) and optimized (right) binning approach for phantom and patient data for patients with significant longer exhale phase. (a) shows the whole breathing curve for phantom or patient data. In (b), the part of the significant longer expiration is zoomed in and demonstrates the distribution of the binning points for different types of binning. Due to missing projection data for inspiration, the scan area before first maximum is used for reconstruction with standard binning. The 0% and 40% of the inspiration share the same data, as the minimum of breathing curve is not detected due to the missing inhalation portion of the cycle. For the optimized reconstruction, the same projection data points are used for both expiration and inspiration. Resulting artifacts due to mismatched breathing phases are shown in (c) and marked with red arrows. For the optimized binning approach for too long exhale phases a significant increase in image quality can be observed even if there are still artifacts due to hysteresis motion, as there is an offset between the paths of respiratory phases. (For interpretation of the references to colour in this figure legend, the reader is referred to the web version of this article.)

reconstructions were statistically significant (p-value < 0.001), except of at 40% inspiration (p- value > 0.05).

3.2. Patient data

Regarding patient data, the standard selection of the binning points was not appropriate for significantly longer breathing cycle. These did not match with the binning points of the breathing curves of the previous and following detector positions, resulting in 4DCT artifacts in the liver (see Fig. 5, left). By optimizing the selection of binning points, these artifacts could be avoided (see Fig. 5, right). Hence, a significant improvement in image quality was achieved. However, unlike in the phantom study, no conclusion about the geometric accuracy and imaging fidelity of the reconstructions could be made, since a ground truth did not exist.

4. Discussion

In the present study, an algorithm for optimized raw data selection in the presence of strong breathing irregularities aiming to improve image quality as well as geometric accuracy was evaluated. It seamlessly followed previous *in-silico*, phantom-based and clinical studies, which demonstrated a significant improvement in image quality with i4DCT compared to conventional algorithms [13–16,25]. Although 74% of the phantom [16] and 89% of the patient scans [25] were described as (nearly) artifacts-free with i4DCT compared to 13% and 25% with conventional algorithms, respectively, image artifacts still occurred in some cases, especially for single significant longer breathing cycles or breathing amplitudes $< 50\%$ of the reference cycle. For radiation protection reasons, a scan is currently stopped at a distinct z-position when reaching a maximum scan time t_{max}, resulting in insufficient information for image reconstruction. Approximately 2–5% of all scans are affected. Artifacts like double or incomplete structures occur (see Fig. 5c, left).

Various strategies have been developed to avoid artifacts. One possibility is to repeat the whole 4DCT or at least individual parts, resulting in an additional radiation exposure [8]. A new deep-learning based inpainting approach can detect missing data artifacts and restore anatomically correct image information [26]. Other conventional image post-processing approaches currently address only artifacts due to irregular breathing amplitudes [27–29].

The new approach for optimized raw data selection is intended to improve image quality without additional dose exposure. Thereby, missing or incorrect inspiration data is replaced by respective expiration data. The current study investigated its effect on geometric accuracy and image quality using phantom and patient measurements. Since the algorithm, by definition, does not address hysteresis in motion trajectory, such motions were of particular interest.

The phantom study demonstrated that 4DCT-related step artifacts, resulting from missing inspiration data, were avoided by using the optimized binning in comparison to standard reconstruction. Significant improvements of image quality as well as geometrical accuracy were achieved. Even for hysteresis motions, only small volume deviations were found. Considering the Dice coefficient, it can be demonstrated that even with the new binning approach problems due to hysteresis motion still occur. Although significantly better results were obtained for the optimized binning approach considering one- and three-dimensional motion compared to standard reconstruction, the results for hysteresis motion were almost the same (median of 0.918 ± 0.148 for standard and 0.915 ± 0.075 optimized reconstruction) with respect to both techniques. By replacing the missing information with expiration data, the algorithm ignores the differences in the tumor trajectory, as indicated by the low Dice coefficient.

A significant reduction of artifacts could be observed in the patient case, resulting in a higher image quality. However, no statement could be made about the accuracy, since there was no ground truth. Different research groups analyzed the trajectories of lung tumors and metastasis of patients. Seppenwoolde *et al.* showed hysteresis in up to 50% of the patients with differences in the trajectories between 1 mm and 5 mm [23]. According to [30], 75% of the patients have differences of ≤ 3 mm.

To draw qualitative and quantitative conclusions about the impact of the optimized approach on treatment planning and dose calculation, a comprehensive study with a ground truth is necessary. In a follow-up patient study, a termination of CT acquisition at a defined table position will have to be simulated to artificially generate missing inspiration data. In this way, not only a patient-specific reference scan will be provided, but the position of missing data can be freely chosen and thus placed in the GTV, resulting in a worst case scenario. It is considered essential to investigate the effect of optimized binning on GTV and ITV definition, dose calculation and Average and MaxIP reconstructions.

Nevertheless, considering the very good correction of image artifacts, the introduction of the optimized binning approach will need increased clinical attention since the clinical staff may no longer be able to distinguish between corrected and uncorrected scans. This results in a perceived certainty, which could lead to contouring errors if this issue is not taken into account. A labelling of the altered slices could help to avoid potential mistakes.

In summary, the optimized binning selection was proven to reduce 4DCT-related artifacts due to missing projection data without further dose exposure, avoiding potentially delays in therapy start. However, it is recommended to label the corrected CT slices to decide individually whether specific measures, e.g. additional safety margins in the affected z-position, have to be taken.

Declaration of Competing Interest

The authors declare the following financial interests/personal relationships which may be considered as potential competing interests: The Universitätsklinikum Erlangen and the Department of Radiation Oncology have institutional research grants with Siemens Healthcare GmbH.

Acknowledgements

We acknowledge financial support by Deutsche Forschungsgemeinschaft and Friedrich-Alexander-Universität Erlangen-Nürnberg within the funding programme “Open Access Publication Funding”.

Appendix A. Supplementary data

A – Videos of 4DCT scans reconstructed with standard and optimized raw data selection algorithm Videos of 4DCT scans without breathing pause (A.1) as well as with breathing pause reconstructed with standard reconstruction (A.2.) and with optimized raw data selection algorithm (A.3) for three-dimensional movement with and without hysteresis motion are available.

Supplementary data to this article can be found online at https://doi.org/10.1016/j.phro.2024.100584.

References

[1] Brandner ED, Chetty IJ, Giaddui TG, Xiao Y, Huq MS. Motion management strategies and technical issues associated with stereotactic body radiotherapy of thoracic and upper abdominal tumors: A review from NRG oncology. Med Phys 2017;44:2595–612. https://doi.org/10.1002/mp.12227.

[2] Korreman S, Persson G, Nygaard D, Brink C, Juhler-Nottrup T. Respiration-correlated image guidance is the most important radiotherapy motion management strategy for most lung cancer patients. Int J Radiat Oncol 2012;83:1338–43. https://doi.org/10.1016/j.ijrobp.2011.09.010.

[3] Landberg T, Chavaudra J, Dobbs J, Gerard JP, Hanks G, Horiot JC, et al. ICRU Report 62: Prescribing, Recording and Reporting Photon Beam Therapy (Supplement to ICRU Report 50), Reports of the International Commission on Radiation Units and Measurements 1999; os-32(1): 1–52.

[4] Schmitt D, Blanck O, Gauer T, Fix MK, Brunner TB, Fleckenstein J, et al. Technological quality requirements for stereotactic radiotherapy : Expert review

group consensus from the DGMP Working Group for Physics and Technology in Stereotactic Radiotherapy. Strahlenther Onkol 2020;196(5):421–43. https://doi.org/10.1007/s00066-020-01583-2.
[5] Persson GF, Nygaard DE, Brink C, Jahn JW, Munck af Rosenschöld P, Specht L, et al. Deviations in delineated GTV caused by artefacts in 4DCT. Radiother Oncol 2010;96(61–6). https://doi.org/10.1016/j.radonc.2010.04.019.
[6] Mutaf YD, Antolak JA, Brinkmann DH. The impact of temporal inaccuracies on 4DCT image quality. Med Phys 2007;34:1615–22. https://doi.org/10.1118/1.2717404.
[7] Langner UW, Keall PJ. Prospective displacement and velocity-based cine 4D CT. Med Phys 2008;35:4501–12. https://doi.org/10.1118/1.2977539.
[8] Castillo SJ, Castillo R, Castillo E, Pan T, Ibbott G, Balter P, et al. Evaluation of 4D CT acquisition methods designed to reduce artifacts. J Appl Clin Med Phys 2015;16:4949. https://doi.org/10.1120/jacmp.v16i2.4949.
[9] Keall PJ, Mageras GS, Balter JM, Emery RS, Forster KM, Jiang SB, et al. The management of respiratory motion in radiation oncology report of AAPM Task Group 76. Med Phys 2006;33:3874–900. https://doi.org/10.1118/1.2349696.
[10] Sentker T, Schmidt V, Ozga AK, Petersen C, Madesta F, Hofmann C, et al. 4D CT image artifacts affect local control in SBRT of lung and liver metastases. Radiother Oncol 2020;148:229–34. https://doi.org/10.1016/j.radonc.2020.04.006.
[11] Keall PJ, Vedam SS, George R, Williamson JF. Respiratory regularity gated 4D CT acquisition: concepts and proof of principle. Australas Phys Eng S 2007;30:211. https://doi.org/10.1007/BF03178428.
[12] Martin S, O'Brien R, Hofmann C, Keall P, Kipriditis J. An in silico performance characterization of respiratory motion guided 4DCT for high-quality low-dose lung cancer imaging. Phys Med Biol 2018;63:155012. https://doi.org/10.1088/1361-6560/aaceca.
[13] Werner R, Sentker T, Madesta F, Gauer T, Hofmann C. Intelligent 4D CT sequence scanning (i4DCT): Concept and performance evaluation. Med Phys 2019;46:3462–74. https://doi.org/10.1002/mp.13632.
[14] Werner R, Sentker T, Madesta F, Schwarz A, Vornehm M, Gauer T, et al. Intelligent 4D CT sequence scanning (i4DCT): First scanner prototype implementation and phantom measurements of automated breathing signal-guided 4D CT. Med Phys 2020;47:2408–12. https://doi.org/10.1002/mp.14106.
[15] Szkitsak J, Werner R, Fernolendt S, Schwarz A, Ott OJ, Fietkau R, et al. First clinical evaluation of breathing controlled four-dimensional computed tomography imaging. Phys Imaging Radiat Oncol 2021;20:56–61. https://doi.org/10.1016/j.phro.2021.09.005.
[16] Werner R, Szkitsak J, Sentker T, Madesta F, Schwarz A, Fernolendt S, et al. Comparison of intelligent 4D CT sequence scanning and conventional spiral 4D CT: a first comprehensive phantom study. Phys Med Biol 2021;66. https://doi.org/10.1088/1361-6560/abc93a.
[17] Szkitsak J, Karius A, Hofmann C, Fietkau R, Bert C, Speer S. Quality assurance of a breathing controlled four-dimensional computed tomography algorithm. Phys Imaging Radiat Oncol 2022;23:85–91. https://doi.org/10.1016/j.phro.2022.06.007.
[18] Werner R, Hofmann C, Mucke E, Gauer T. Reduction of breathing irregularity-related motion artifacts in low-pitch spiral 4D CT by optimized projection binning. Radiat Oncol 2017;12:100. https://doi.org/10.1186/s13014-017-0835-7.
[19] Computerized Imaging Reference Systems: CIRS Motion Control - User Manual. 2017 14.02.2022]. Available from: http://www.cirsinc.com/wp-content/uploads/2019/11/CIRS_Motion_Control_User_Manual.pdf. http://www.cirsinc.com/wp-content/uploads/2019/11/CIRS_Motion_Control_User_Manual.pdf.
[20] Lambrecht M, Sonke J-J, Nestle U, Peulen H, Weber DC, Verheij M, et al. Quality assurance of four-dimensional computed tomography in a multicentre trial of stereotactic body radiotherapy of centrally located lung tumours. Phys Imaging Radiat Oncol 2018;8:57–62. https://doi.org/10.1016/j.phro.2018.10.003.
[21] Sande EPS, Acosta Roa AM, Hellebust TP. Dose deviations induced by respiratory motion for radiotherapy of lung tumors: Impact of CT reconstruction, plan complexity, and fraction size. J Appl Clin Med Phys 2020;21:68–79. https://doi.org/10.1002/acm2.12847.
[22] Lujan AE, Larsen EW, Balter JM, Ten Haken RK. A method for incorporating organ motion due to breathing into 3D dose calculations. Med Phys 1999;26:715–20. https://doi.org/10.1118/1.1609057.
[23] Seppenwoolde Y, Shirato H, Kitamura K, Shimizu S, van Herk M, Lebesque JV, et al. Precise and real-time measurement of 3D tumor motion in lung due to breathing and heartbeat, measured during radiotherapy. Int J Radiat Oncol 2002;53:822–34. https://doi.org/10.1016/S0360-3016(02)02803-1.
[24] Brock KK, Mutic S, McNutt TR, Li H, Kessler ML. Use of image registration and fusion algorithms and techniques in radiotherapy: Report of the AAPM Radiation Therapy Committee Task Group No. 132. Med Phys 2017; 44:e43-e76. https://doi.org/10.1002/mp.12256.
[25] Werner R, Szkitsak J, Madesta F, Büttgen L, Wimmert L, Sentker T, et al. Clinical application of breathing-adapted 4D CT: image quality comparison to conventional 4D CT. Strahlenther Onkol 2023;199:686–91. https://doi.org/10.1007/s00066-023-02062-0.
[26] Madesta F, Sentker T, Gauer T, Werner R. Deep learning-based conditional inpainting for restoration of artifact-affected 4D CT images. Med Phys 2023:1–18. https://doi.org/10.1002/mp.16851.
[27] Shao W, Pan Y, Durumeric OC, Reinhardt JM, Bayouth JE, Rusu M, et al. Geodesic density regression for correcting 4DCT pulmonary respiratory motion artifacts. Med Image Anal 2021;72:102140. https://doi.org/10.1016/j.media.2021.102140.
[28] He T, Xue Z, Nitsch PL, Teh BS, Wong ST. Helical mode lung 4D-CT reconstruction using Bayesian model. Med Image Comput Comput Assist Interv 2013;16(Pt 3):33–40. https://doi.org/10.1007/978-3-642-40760-4_5.
[29] Han D, Bayouth J, Bhatia S, Sonka M, Wu X. In: Motion Artifact Reduction in 4D Helical CT: Graph-Based Structure Alignment. Berlin Heidelberg: Medical Computer Vision Recognition Techniques and Applications in Medical Imaging; 2011. p. 63–73.
[30] Dhont J, Vandemeulebroucke J, Burghelea M, Poels K, Depuydt T, Van Den Begin R, et al. The long- and short-term variability of breathing induced tumor motion in lung and liver over the course of a radiotherapy treatment. Radiother Oncol 2018;126:339–46. https://doi.org/10.1016/j.radonc.2017.09.001.